Robust Design for the Lower Extremity Exoskeleton Under a Stochastic Terrain by Mimicking Wolf Pack Behaviors

ZHONGLAI WANG[1,2], **SHUI YU**[1,2], **LEO YI CHEN**[3], **(Senior Member, IEEE), AND YUN LI**[3,4]

[1]School of Mechanical and Electrical Engineering, University of Electronic Science and Technology of China, Chengdu 611731, China
[2]Center for System Reliability and Safety, University of Electronic Science and Technology of China, Chengdu 611731, China
[3]School of Computer Science and Network Security, Dongguan University of Technology, Dongguan 523808, China
[4]Faculty of Engineering, University of Strathclyde, Glasgow G1 1XJ, U.K.

Corresponding authors: Zhonglai Wang (wzhonglai@uestc.edu.cn) and Leo Yi Chen (leo.chen@ieee.org)

ABSTRACT While kinematics analysis plays an important role in studying human limb motions, existing methods (namely, direct and inverse kinematics) have their deficiencies. To improve, this paper develops a robust design method using artificial intelligence and applies it to the lower extremity exoskeleton design under a stochastic terrain. An inverse kinematic model is first built considering the impact on human's comfort from the stochastic terrain. Then, a robust design model is constructed based on the inverse kinematic model, where the design framework mimics wolf pack behaviors and the robust design problem is thus solved for keeping probabilistic consistency between the exoskeleton and its wearer. A case study validates the effectiveness of the developed robust method and algorithm, which ensures walking comfort under the stochastic terrain within the validity of simulations.

INDEX TERMS Wolf packs, inverse kinematics, lower extremity exoskeleton, robust design, stochastic terrain.

I. INTRODUCTION

Kinematics analysis plays an important role in studying motions for human limbs. Direct kinematics and inverse kinematics are usually the two approaches adopted. Direct kinematics maps the joints space that is often used in motion study to the Cartesian space that is often used to obtain the position of the end-effector. On contrast, inverse kinematics is expressed as a mapping from the Cartesian space to the joints space for pursuing the positions of the joints. Hence inverse kinematics is used for finding the joint angle trajectories while satisfying the constraints of the end-effector, which has been widely used in computer animation and simulation of articulated figures, motion capture and task feasibility studies [1].

Existing inverse kinematic methods assume that the positions of joints are deterministic without considering randomness and variability. However, due to the presence of uncertainties in systems and environments [2]–[4], it is necessary to handle the effect of randomness and variability

from the end-effector to the joints during the procedure of inverse kinematics. For example, during rehabilitation training, the effects of randomness on foot from a stochastic terrain should be included for the inverse kinematic problem, even though sensors are used. At present, challenges exist, as inverse kinematics requires solving highly non-linear equations, such as using a geometric [5], algebraic [6] or iterative [7] method. Closed-form solutions for the first three joints should exist geometrically in the geometric method while the algebraic method could not guarantee the closed-form solutions.

In arriving at a solution, an iterative method could be used, but this is prone to converging to one feasible solution, depending on the starting point, that is suboptimal. To address this issue, researchers have studied the use of artificial intelligence based methods. Owing to its intuitive 'black-box' learning characteristics, the artificial neural network has been used for improving the training accuracy and reducing the training time [8]–[12]. For instance, Bingul and Ertunc [8]

Z. Wang *et al.*: Robust Design for the Lower Extremity Exoskeleton Under a Stochastic Terrain by Mimicking WP Behaviors

IEEE *Access*

have used the backpropagation algorithm to solve inverse problems of the industrial robot manipulator with high accuracy; Köker [10] has optimized the neural network using a genetic algorithm for a six-joint Stanford robotic manipulator with minimized error of the end-effector.

Artificial intelligence based optimization methods, such as the genetic algorithm [13], [14], artificial bees algorithm [15], and particle swarm optimization algorithm [16] are the recent focus in directly solving optimization models of the inverse kinematic problems. Tabandeh *et al.* [13] have used an adaptive niching genetic algorithm to find multiple solutions of the inverse kinematics. Momani *et al.* [14] have employed the continuous genetic algorithm to solve the optimization model built for the inverse kinematic problem for minimizing the accumulative path deviation in the absence of any obstacles. Pham *et al.* [15] have used artificial bees algorithm for training multi-layer perceptron neural networks to solve the inverse kinematic problem of an articulated robot manipulator arm. Huang *et al.* [16] have proposed an optimization method for the inverse kinematics of 7 degree-of-freedom robotic manipulators based on the particle swarm optimization algorithm.

Despite much effort made in finding tractable solutions to inverse kinematic problems, the randomness or variability inherent in systems and working environment affecting the quality of motion has been rarely been taken into consideration so far. Hence, this paper aims to develop a robust design method for inverse kinematic problems of the human lower extremity exoskeleton, such that joints can randomly respond to a stochastic terrain for realizing high robustness. In particular, the paper addresses: (1) the inverse kinematic model of the lower extremity exoskeleton under the stochastic terrain is constructed; (2) a robust design model based on the inverse kinematic model under the stochastic terrain for increasing the comfort of the wearer is presented; (3) a multi-objective optimization framework for solving the robust design based on the developed artificial wolf pack algorithm (AWPA) for ensuring the robustness and consistence of the motion of joints. Meanwhile, the paper will provide design results for gait planning for rehabilitation training and wearable lower extremity exoskeleton under the stochastic terrain.

The remainder of the paper is organized as follows. The determination method of the target position of the end-effector under the stochastic terrain is analyzed in Section 2. Section 3 presents the robust design model for the inverse kinematic problem under a stochastic terrain. Section 4 details the framework for solving the robust design based on AWPA. Results and discussions of a case study are provided in Section 5. Conclusions are drawn in Section 6.

II. DETERMINATION OF TARGET POSITION OF THE END-EFFECTOR UNDER A STOCHASTIC TERRAIN

The lower extremity exoskeleton is assumed to be consisted of three joints and connected with rigid links for the direct and inverse kinematic problems. For the lower extremity exoskeleton model, six-degrees-of-freedom (DOF) are considered, *e.g.*: three at the hip joint, one at the knee joint and two at the ankle joint. As shown in Figure 1 [17], a base frame is placed at the center of the pelvis between the hips, namely *base* $X_0Y_0Z_0$; the hip frames are *circumduction* $X_1Y_1Z_1$, *adduction-abduction* $X_2Y_2Z_2$, and *flexion-extension* $X_3Y_3Z_3$; the knee joint frame is *flexion-extension* $X_4Y_4Z_4$; the ankle frames are *dorsiflexion-plantarflexion* $X_5Y_5Z_5$ and *inversion-eversion* $X_6Y_6Z_6$; the end-effector is positioned at the tip of the longest toe, $X_7Y_7Z_7$.

The corresponding Denavit–Hartenberg (D-H) parameters of the lower extremity exoskeleton are summarized in Table 1 [17]. The position of the end-effector can be obtained with the defined frames in Figure 1 and the corresponding parameters in Table 1 based on the D-H transformation. The D-H transformation matrix is provided as (1), as shown at the bottom of this page, where

$$
\begin{aligned}
s_i &= \sin(\beta_i); \\
c_i &= \cos(\beta_i); \\
c_{ij} &= \cos(\beta_i + \beta_j); \\
s_{ij} &= \sin(\beta_i + \beta_j); \\
c_{ijk} &= \cos(\beta_i + \beta_j + \beta_k); \\
s_{ijk} &= \sin(\beta_i + \beta_j + \beta_k).
\end{aligned}
$$

The symbols x, y and z in Eqs. (2) - (4), as shown at the bottom of this page, respectively represent the position of the end-effector in the x, y and z directions.

The human walking cycle begins with the start of the stance phase (foot on the ground) at the heel strike followed by the toe-off and swing phase (foot off the ground), shown

$$
\begin{aligned}
{}^0_7T &= {}^0_1T\,{}^1_2T\,{}^2_3T\,{}^3_4T\,{}^4_5T\,{}^5_6T\,{}^6_7T \\[4pt]
&= \begin{bmatrix}
-s_1s_2c_6c_{345} + c_1c_6s_{345} + s_6s_1c_2 & s_1s_2s_6s_{345} - c_1s_6s_{345} - s_1c_2c_6 & -c_1s_2s_{345} - c_1c_{345} & x \\
c_1s_2c_6c_{345} + s_1c_6s_{345} + c_1c_2s_6 & -c_1s_2s_6c_{345} - s_1s_6s_{345} + c_1c_2c_6 & c_1s_2s_{345} - s_1c_{345} & y \\
-c_2c_6c_{345} - s_2s_6 & -c_2s_6c_{345} - s_2c_6 & 0 & z \\
0 & 0 & 0 & 1
\end{bmatrix}
\end{aligned} \tag{1}
$$

$$
x = -l_1(c_1s_3 - s_1s_2c_3) - l_2(c_1c_{34} + s_1s_2s_{34}) - l_3(s_1s_2s_{345} + c_1c_{345}) + a_0 \tag{2}
$$

$$
y = -l_1(s_1s_3 + c_1s_2c_3) + l_2(c_1s_2s_{34} - s_1c_{34}) + l_3(c_1s_2s_{345} - s_1c_{345}) \tag{3}
$$

$$
z = -l_1c_2c_3 + l_2c_2s_{34} + l_3c_2s_{345} + d_0 \tag{4}
$$

IEEE *Access*

Z. Wang *et al.*: Robust Design for the Lower Extremity Exoskeleton Under a Stochastic Terrain by Mimicking WP Behaviors
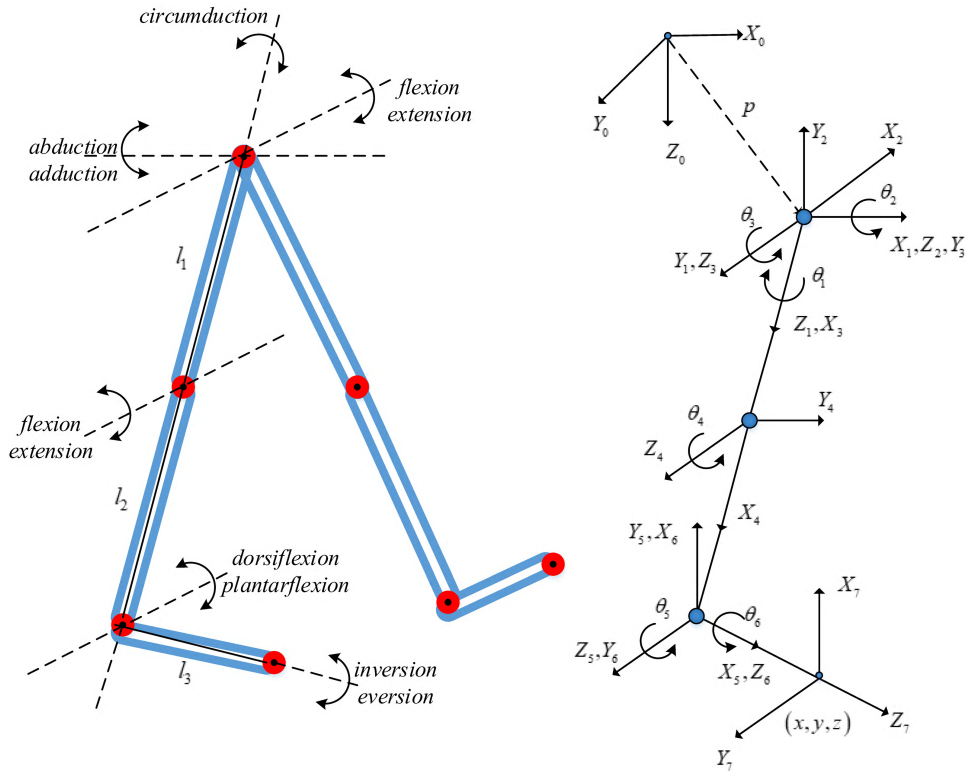

FIGURE 1. Dynamic frames for lower extremity exoskeleton [17].

TABLE 1. D-H parameters of the lower extremity exoskeleton [17].

Joint	β_i	Number	α_i	a_i	d_i	θ_i
Base	0	1(0→1)	0	a_0	d_0	0
Hip	(-50) medial rotation/lateral rotation (+40)	2(1→2)	$-90°$	0	0	$\beta_1 + 90°$
Hip	(-20) abduction/adduction (+45)	3(2→3)	$+90°$	0	0	$\beta_2 + 90°$
Hip	(-30) extension/flexion (+120)	4(3→4)	0	l_1	0	β_3
Knee	0 extension/flexion (+150)	5(4→5)	0	l_2	0	$\beta_4 + 90°$
Ankle	(-40) plantarflexion/dorsiflexion (+20)	6(5→6)	$+90°$	0	0	$\beta_5 + 90°$
Ankle	(-35) inversion/eversion (+20)	7(6→7)	0	0	l_3	β_6

in Figure 2. The stance phase occupies 60% over the whole human walking cycle and swing phase for 40%. Because of symmetry of the lower extremity exoskeleton, we will only consider one side of the lower extremity exoskeleton, e.g. the right side. The time period for the stance phase is defined as $[t_{hs}, t_{t0}]$.

The position of the end-effector is theoretically the same as that calculated from D-H transformation based on Eqs. (2) - (4). However, while walking during the stance phase, the foot should keep touch with the terrain possessing randomness, which will affect the actual position of the end-effector. Therefore, the randomness from the stochastic terrain should be considered for calculating the actual position of the end-effector when handling inverse kinematic problems. The actual position of the end-effector at the given time point t_{hi}

could be expressed by

$$x^T = x + q(vt_{hi}, x') \tag{5}$$
$$y^T = y + q(vt_{hi}, y') \tag{6}$$
$$z^T = z + q(vt_{hi}, z') \tag{7}$$

where $q(vt_{hi}, x')$, $q(vt_{hi}, y')$ and $q(vt_{hi}, z')$ are random variables for describing the stochastic terrain at the given time point t_{hi}. When the whole stance phase is accounted for, x, y, z and $q(vt_{hi}, x')$, $q(vt_{hi}, y')$, $q(vt_{hi}, z')$ are time-varying, and therefore the general case for Eqs. (5) - (7) could be

$$x^T(t) = x(t) + q(vt, x') \tag{8}$$
$$y^T(t) = y(t) + q(vt, y') \tag{9}$$
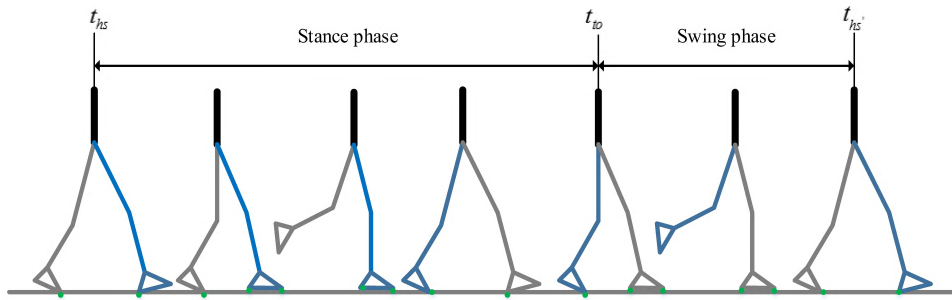$$z^T(t) = z(t) + q(vt, z') \tag{10}$$

Z. Wang *et al.*: Robust Design for the Lower Extremity Exoskeleton Under a Stochastic Terrain by Mimicking WP Behaviors

IEEE *Access*

FIGURE 2. Human walking cycle [18].

Eqs. (8) - (10) could be extended for including other inherent or outside uncertainties, where $q(vt, x')$, $q(vt, y')$ and $q(vt, z')$ could be quantified from the stochastic terrain. Studies show that the terrain roughness follows or approximately follows the ergodic stationary stochastic process [19]. In engineering practices, the terrain roughness could be qualified with the power spectral density

$$G_x(n) = G_x(n_0)\left(\frac{n}{n_0}\right)^w \qquad (11)$$

where $G_x(n_0)$ is the coefficient of the terrain roughness; n_0 is the reference space frequency; w is the frequency index.

A human walks in the time domain. Therefore, the terrain roughness model is transformed from the space domain to the time domain based on the Flourier transformation

$$q(vt) = \frac{1}{N}\sum_{k=0}^{N}\sqrt{\frac{N}{2v\Delta t}G_q(n_k)\left(\frac{n_k}{n_0}\right)^w}e^{j\varphi_k}e^{\frac{2\pi kmj}{N}},$$
$$(m = 0, 1, 2, \ldots, N-1) \qquad (12)$$

where N is the number of samples; φ_k is a random variable; Δt denotes the time step, which is consistent with the discretization step of the human gait; v is the velocity of human walking; n_k defines the space frequency. In the latter example for the inverse kinematic problem, the parameters are set to $G_q(n_k) = 16 \times 10^{-6}$; $n_0 = 0.1$; $\varphi_k \in [0, 2\pi]$; $n_k = 0.01$.

III. ROBUST OPTIMIZATION MODEL FOR THE INVERSE KINEMATIC PROBLEM UNDER A STOCHASTIC TERRAIN

The randomness of the joints will react to the randomness from the position of the end-effector for ensuring the consistency. Without losing its generality, the stochastic processes $\beta_i(t)$ $(i = 1, 2, \cdots, 5)$ are the alternatives to describe the random motion during the stance phase.

With the D-H transformation in the direct kinematics, the mapping from the motion of the joints to the position of the end-effector under randomness at the given time point t_{hi} could be represented as

$$x(t_{hi}) = f_1(\beta_1(t_{hi}), \beta_2(t_{hi}), \beta_3(t_{hi}), \beta_4(t_{hi}), \beta_5(t_{hi})) \qquad (13)$$

$$y(t_{hi}) = f_2(\beta_1(t_{hi}), \beta_2(t_{hi}), \beta_3(t_{hi}), \beta_4(t_{hi}), \beta_5(t_{hi})) \qquad (14)$$

$$z(t_{hi}) = f_3(\beta_1(t_{hi}), \beta_2(t_{hi}), \beta_3(t_{hi}), \beta_4(t_{hi}), \beta_5(t_{hi})) \qquad (15)$$

$f_1(\cdot), f_2(\cdot)$ and $f_3(\cdot)$ in Eqs. (13) - (15) could be illustrated with the mapping in Eqs. (2) - (4) respectively in detail. However, $\beta_i(t_{hi})$ $(i = 1, 2, \cdots, 5)$ in Eqs. (13) - (15) are random variables while they are deterministic variables in Eqs. (2) - (4).

Because of the complexity of functions $x(t_{hi})$, $y(t_{hi})$, and $z(t_{hi})$, the second order Taylor expansion is implemented. The mean and standard deviation of $x(t_{hi})$, $y(t_{hi})$, and $z(t_{hi})$ can be derived by extending the functions at the mean values $(\bar{\beta}_1(t_{hi}), \bar{\beta}_2(t_{hi}), \bar{\beta}_3(t_{hi}), \bar{\beta}_4(t_{hi}), \bar{\beta}_5(t_{hi}))$, (16)–(21), as shown at the bottom of the next page, where $E(\cdot)$ and $D(\cdot)$ denote the mean value and standard deviation; $\widehat{\beta}_i(\cdot)$ denotes the standard deviation of $\beta_i(\cdot)$.

The main objective is comfortable and energy-efficient when designing the exoskeleton. The objective can be realized by minimizing both the difference between the actual and targeted mean values, and the standard deviation of the random motion of the joints at the same time. In other words, the motion of each joint should be robust. Therefore, it is necessary to construct a robust design model for obtaining the optimal solutions. At the given time point t_{hi}, the design variables are expressed as the vector

$$DV = \begin{pmatrix} \bar{\beta}_1(t_{hi}), \bar{\beta}_2(t_{hi}), \bar{\beta}_3(t_{hi}), \bar{\beta}_4(t_{hi}), \bar{\beta}_5(t_{hi}), \\ \widehat{\beta}_1(t_{hi}), \widehat{\beta}_2(t_{hi}), \widehat{\beta}_3(t_{hi}), \widehat{\beta}_4(t_{hi}), \widehat{\beta}_5(t_{hi}) \end{pmatrix};$$

the objective functions f_1 and f_2 form the robustness index; the consistency between the targeted and the actual position of the end-effector is considered as constraints. The CGA (Clinical Gait Analysis) data measured from the experiments is treated as the targeted mean value for constructing the objective function as the robustness index. Then the robust design model is provided as

$$\min f_1 = \sum_{i=1}^{5}\left|\bar{\beta}_i(t_{hi}) - \bar{\beta}_i^T(t_{hi})\right|$$

$$f_2 = \sum_{i=1}^{5}\widehat{\beta}_i(t_{hi})$$

$$s.t. \ g_1 = E(x(t_{hi})) - E\left(x^T(t_{hi})\right) = 0$$

IEEE *Access*

Z. Wang *et al.*: Robust Design for the Lower Extremity Exoskeleton Under a Stochastic Terrain by Mimicking WP Behaviors
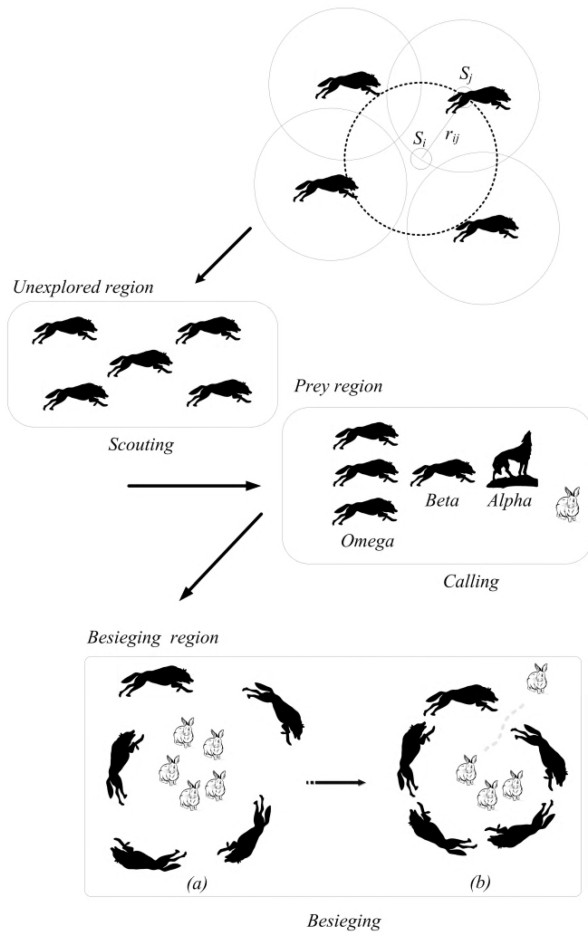
FIGURE 3. A wolf pack's dynamic behaviours.

$$g_2 = E\left(y\left(t_{hi}\right)\right) - E\left(y^T\left(t_{hi}\right)\right) = 0$$

$$g_3 = E\left(z\left(t_{hi}\right)\right) - E\left(z^T\left(t_{hi}\right)\right) = 0$$

$$g_4 = D\left(y\left(t_{hi}\right)\right) - D\left(y^T\left(t_{hi}\right)\right) = 0$$

$$\hat{\beta}_i\left(t_{hi}\right) \geq 0; \quad i = 1, \ldots, 5 \tag{22}$$
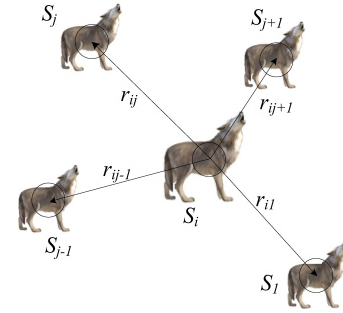

FIGURE 4. AW state updating.

The similar robust design model could be built for other time points during the whole stance phase. However, the optimal results for each time points will fluctuate around the actual motion of joints. The smooth method could be implemented for keeping the consistency with the practical case.

Obviously, Eq. (22) is a multi-objective optimization problem. Many methods have been developed for solving multi-objective optimization problems, such as the non-dominated sorting genetic algorithm (NSGA) [20], the niched-Pareto genetic algorithm (NPGA) [21], the nondominated sorting genetic algorithm II (NSGA-II) [22], etc. Generally, the designer could make trade-offs within this set under practical requirements by focusing the set of Pareto front choices but with an unclear indication of optimal diversities for final decision-making. AWPA could provide users with a recommendation list of optimal ranking and optimal trend indications with different risk tolerance [23]. The framework based on the AWPA for solving Eq. (22) will be proposed in Section 4 effectively.

IV. FRAMEWORK FOR ROBUST DESIGN MIMICKING A WOLF PACK

A. DYNAMIC BEHAVIORS OF A WOLF PACK

Wolves are always regarded as one of the smartest species on Earth, who have developed the capacity to survive in a

$$E\left(x\left(t_{hi}\right)\right) = f_1\left(\overline{\beta}_1\left(t_{hi}\right), \overline{\beta}_2\left(t_{hi}\right), \overline{\beta}_3\left(t_{hi}\right), \overline{\beta}_4\left(t_{hi}\right), \overline{\beta}_5\left(t_{hi}\right)\right) + \frac{1}{2}\sum_{i=1}^{5}\left(\left.\frac{\partial^2 f_1}{\partial\left[\beta_i\left(t_{hi}\right)\right]^2}\right|_{\beta=\overline{\beta}\left(t_{hi}\right)} \hat{\beta}_i\left(t_{hi}\right)\right) \tag{16}$$

$$D\left(x\left(t_{hi}\right)\right) = \sum_{i=1}^{5}\left(\left.\left(\frac{\partial f_1}{\partial\beta_i\left(t_{hi}\right)}\right)^2\right|_{\beta\left(t_{hi}\right)=\overline{\beta}\left(t_{hi}\right)} \hat{\beta}_i\left(t_{hi}\right)\right) \tag{17}$$

$$E\left(y\left(t_{hi}\right)\right) = f_2\left(\overline{\beta}_1\left(t_{hi}\right), \overline{\beta}_2\left(t_{hi}\right), \overline{\beta}_3\left(t_{hi}\right), \overline{\beta}_4\left(t_{hi}\right), \overline{\beta}_5\left(t_{hi}\right)\right) + \frac{1}{2}\sum_{i=1}^{5}\left(\left.\frac{\partial^2 f_2}{\partial\left[\beta_i\left(t_{hi}\right)\right]^2}\right|_{\beta=\overline{\beta}\left(t_{hi}\right)} \hat{\beta}_i\left(t_{hi}\right)\right) \tag{18}$$

$$D\left(y\left(t_{hi}\right)\right) = \sum_{i=1}^{5}\left(\left.\left(\frac{\partial f_2}{\partial\beta_i\left(t_{hi}\right)}\right)^2\right|_{\beta\left(t_{hi}\right)=\overline{\beta}\left(t_{hi}\right)} \hat{\beta}_i\left(t_{hi}\right)\right) \tag{19}$$

$$E\left(z\left(t_{hi}\right)\right) = f_3\left(\overline{\beta}_1\left(t_{hi}\right), \overline{\beta}_2\left(t_{hi}\right), \overline{\beta}_3\left(t_{hi}\right), \overline{\beta}_4\left(t_{hi}\right), \overline{\beta}_5\left(t_{hi}\right)\right) + \frac{1}{2}\sum_{i=1}^{5}\left(\left.\frac{\partial^2 f_3}{\partial\left[\beta_i\left(t_{hi}\right)\right]^2}\right|_{\beta=\overline{\beta}\left(t_{hi}\right)} \hat{\beta}_i\left(t_{hi}\right)\right) \tag{20}$$

$$D\left(z\left(t_{hi}\right)\right) = \sum_{i=1}^{5}\left(\left.\left(\frac{\partial f_3}{\partial\beta_i\left(t_{hi}\right)}\right)^2\right|_{\beta\left(t_{hi}\right)=\overline{\beta}\left(t_{hi}\right)} \hat{\beta}_i\left(t_{hi}\right)\right) \tag{21}$$

Z. Wang *et al.*: Robust Design for the Lower Extremity Exoskeleton Under a Stochastic Terrain by Mimicking WP Behaviors
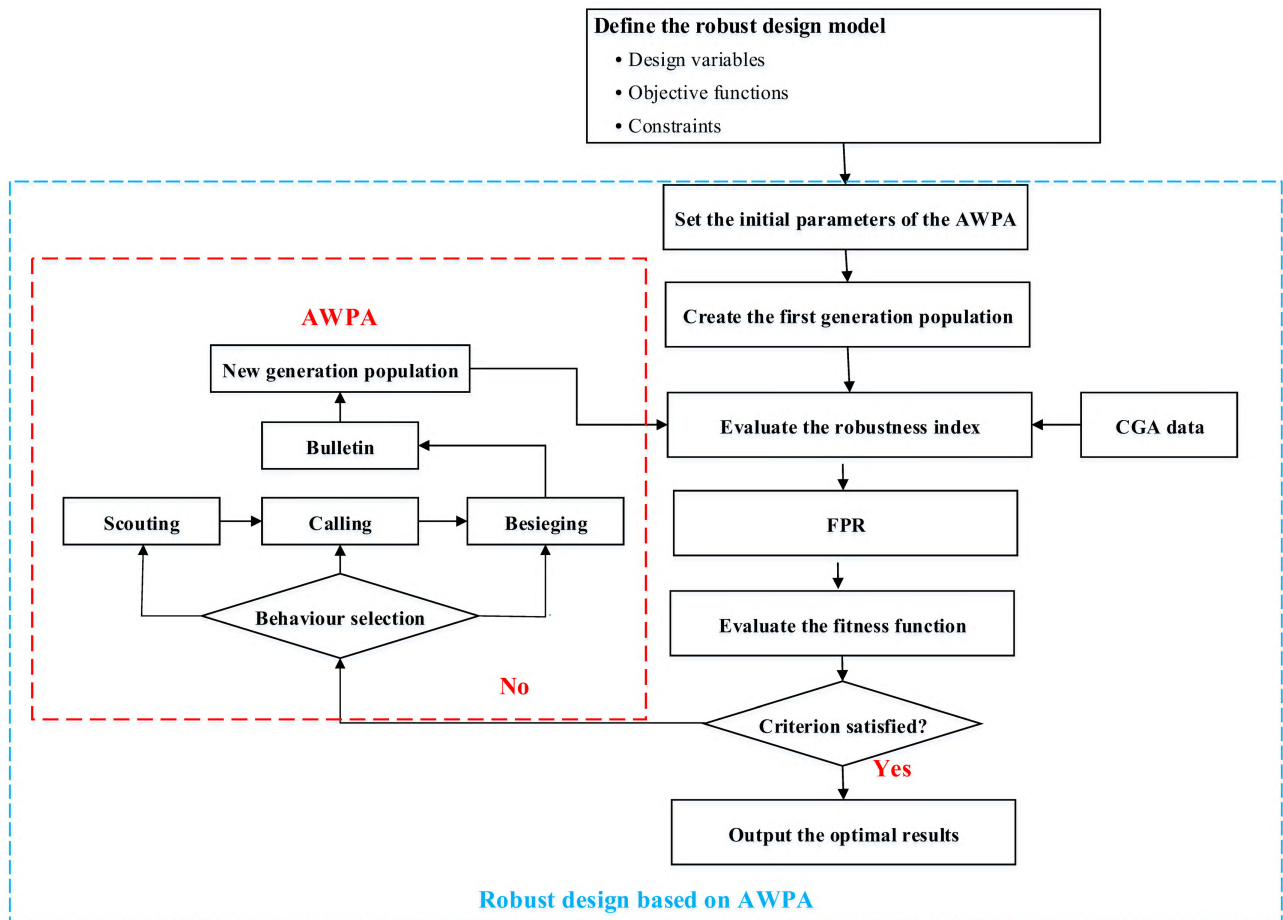
IEEE*Access*

FIGURE 5. Flowchart of the robust design based on AWPA.

wide range of surroundings. The size of a wolf can vary in range, generally, the height varies from 0.6 to 0.95 meters at the shoulder and the weight ranges from 20 to 62 kilograms.

Wolves are gregarious animals who mostly live in packs. A wolf pack (WP) is formed when a male (α) and a female wolf (β) meet and stay together as a mated pair, which has its territory to settle in and raise cubs in most years. Their cubs stay within the WP until they are old enough to leave the home WP, usually at 3 years old, at which point they can start a WP of their own.

Fundamentally, the social structure of a WP can be observed as a permanent core pair plus their continuously dispersing offspring. They have a very strict level of the hierarchy that must be adhered to by all of the members of the pack, which allows the WPs to be able to survive.

A WP has a wide range of complex social behaviours. Basically, there are three main behaviours in a WP's everyday life: *scouting, calling* and *besieging*. As illustrated in Figure 3, there is a leader wolf (usually the α male wolf) in a WP, who is responsible for making a decision according to and commanding the wolves to perform proper actions. The scout wolves are sent out to explore the unknown region (*Scouting*). When the prey has been located in the prey region, scout wolves will report it to the leader wolf and
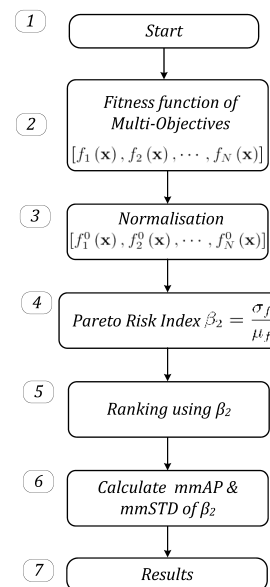

FIGURE 6. Workflow of the fast approach to Pareto-optimal solution recommendation.

communicate with others by howling (*Calling*), then the WP will move towards the scout wolves to start the hunting and capturing (*Besieging*) in the besieging region. In recent years,

IEEE*Access*

Z. Wang *et al.*: Robust Design for the Lower Extremity Exoskeleton Under a Stochastic Terrain by Mimicking WP Behaviors

TABLE 2. Main dimensions of Chinese adults (mm).

	percent (%)	height	thigh length	leg length	foot length	foot width
	1	1543	413	324	233	86
	5	1583	428	338	230	88
18~60	10	1604	436	344	234	90
(years)	50	1678	456	369	247	96
Male	90	1754	496	396	260	102
	95	1775	505	403	264	103
	99	1814	523	419	272	107
	1	1449	387	300	208	78
	5	1484	402	313	213	81
18~55	10	1503	410	319	217	83
(years)	50	1570	438	344	229	88
Female	90	1640	467	370	241	93
	95	1659	476	376	244	95
	99	1697	494	390	251	98

a few researchers have proposed their algorithms inspired by the wolf pack behaviour with different preference, such as: hierarchy of grey wolf [26], wolf pack's hunting strategy [27] and wolf pack's prey search activity [28]–[32].

B. PROCEDURE OF THE AWPA

Inspired by the swarm intelligence of the WP's dynamic behaviours, the AWPA is an artificial intelligence algorithm that firstly simulates the behaviour of an individual artificial wolf (AW) and constructs a WP [23]. Each AW searches its own local optimal solution and passes information to its self-organized WP, and finally achieves the global optimal solution. The work-flow of the AWPA includes 6 steps of operations: (1) initialization; (2) behaviour selection; (3) behaviour of scouting; (4) behaviour of calling; (5) behaviour of besieging and (6) bulletin.

Initialization: in this step, all the parameters will be initialized, and the program is preparing itself for the next steps.

Behaviour Selection: the behaviour selection step takes 'Scouting' as the default behaviour or initial behaviour for each WP. According to the density of prey in this region, the number of companion and the visual conditions.

Scouting: for a certain AW individual k, $S_k = \{s_1, \ldots, s_M\}$ is its finite state set, there is M states that an AW can perform in. Within the AW's visual field, if the current state of this AW is S_i and the next state is S_j, the AW moves from S_i to S_j randomly and check the state updating conditions as stated in Eqs. (23) and (24). As demonstrated in Figure 4, $r_{ij} = |S_j - S_i|$ is the distance between the ith and j^{th} individual AW. $F = f(S)$ is the prey density for this AW, where F is the fitness function, δ is the iteration step, υ is the AW visual

TABLE 3. Parameters for optimization.

	max-generation	200
	population	60
	try number	5
	test number	5
δ	iterate step	0.5
η	crowd	0.618
υ	visual	2.5

constant, and ε is the random moving factor.

$$S_{i+1} = \begin{cases} S_i + \varepsilon \cdot \delta \dfrac{S_j - S_i}{\|S_j - S_i\|} & \text{if } F_j > F_i \\ S_i + \varepsilon \cdot \delta & \text{otherwise} \end{cases} \quad (23)$$

$$S_{i+1} = S_i + \varepsilon \cdot \upsilon \quad (24)$$

Calling: Suppose that the number of this AW's neighbours is γ, the central state is S_c, the prey density is $F_c = f(S_c)$ and η is the crowd factor. Within its visual field $(r_{ij} < \upsilon)$, if $F_c/\gamma > \eta F_i$ and $\eta \geq 1$, the AW implements the central state driven step; otherwise, when the $F_c/\gamma \leq \eta F_i$ or $\eta = 1$, the AW will go on with the scouting behaviour, as expressed in Eq. (23).

$$S_{i+1} = \begin{cases} S_i + \varepsilon \cdot \delta \dfrac{S_c - S_i}{\|S_c - S_i\|} & \text{if } \dfrac{F_c}{\gamma} > \eta F_i \\ \text{Eq. (23)} & \dfrac{F_c}{\gamma} \leq \eta F_i \text{ or } \eta = 1 \end{cases} \quad (25)$$

Besieging: When the AW's companions reach "max" state $S_{\max}$ with the number γ within the neighbourhood, the prey

Z. Wang *et al.*: Robust Design for the Lower Extremity Exoskeleton Under a Stochastic Terrain by Mimicking WP Behaviors
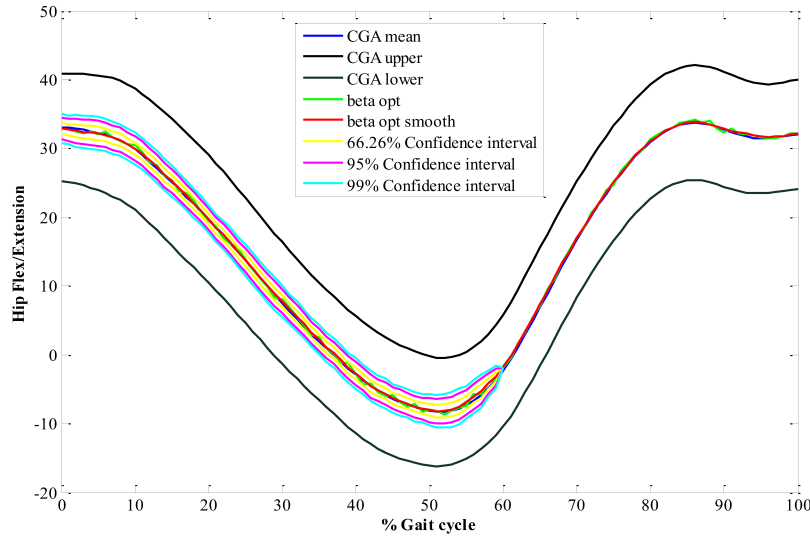
IEEE *Access*

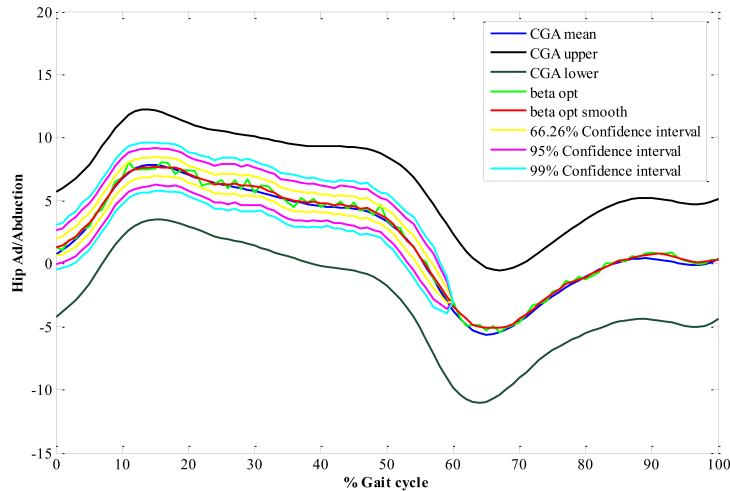**FIGURE 7.** Optimal results for the Hip Flex/Extension.

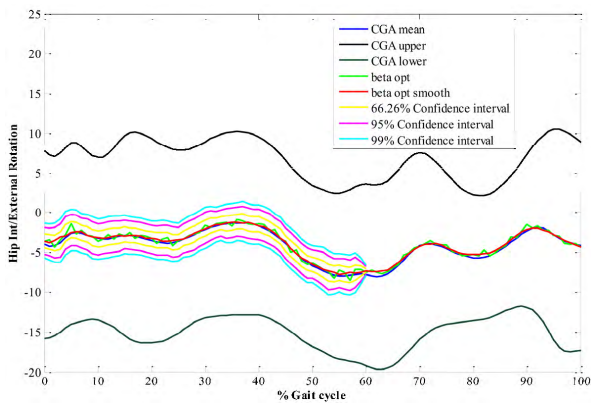**FIGURE 8.** Optimal results for the Hip Ad/Abduction.

FIGURE 9. Optimal results for the Hip Int/External.

density reaches F_{max} at the meantime. As stated in Eq. (25), with the same conditions as Eq. (23), the AW updates its state in highest prey density region; otherwise, the AW will go on with the searching behaviour, as expressed in Eq. (26).

$$S_{i+1} = \begin{cases} S_i + \varepsilon \cdot \delta \dfrac{S_{max} - S_i}{\|S_{max} - S_i\|} & \text{if } \dfrac{F_{max}}{\gamma} > \eta F_i \\ \text{Eq. (23)} & \dfrac{F_{max}}{\gamma} \leq \eta F_i \text{ or } \eta = 1 \end{cases} \quad (26)$$

Bulletin: The bulletin operation is a step to compare each AW's current state S_i with the historical state data, the bulletin data will be replaced and updated only when the current state is better than the last one, as described by Eq. (27).

$$S_{i+1} = \begin{cases} S_j & \text{if } F_j > F_i \\ S_i & \text{otherwise} \end{cases} \quad (27)$$

Termination criteria: If one of the following conditions is satisfied, the algorithm is terminated: (a) the predetermined maximal number of generations is achieved; (b) the fitness for the best WP is no longer rising; and (c) the fitness of the optimal individual reaches a given threshold.
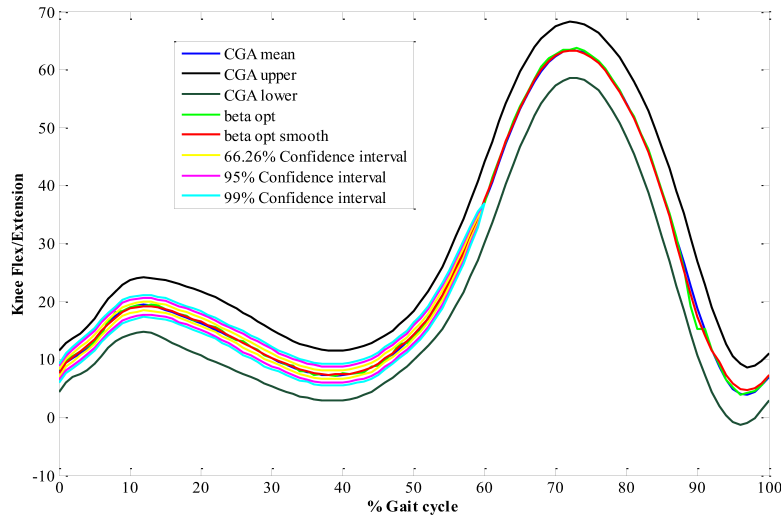
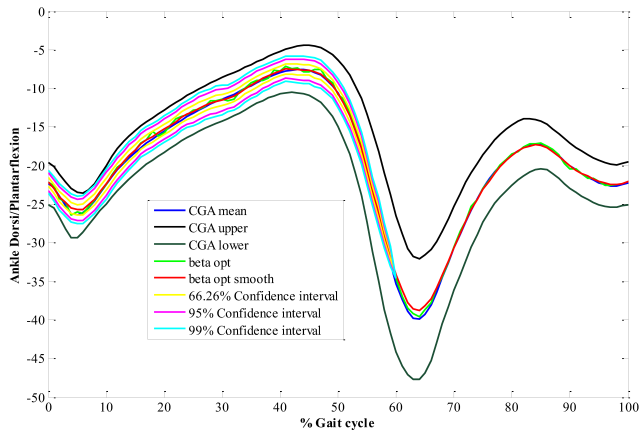**FIGURE 10.** Optimal results for the Knee Flex/Extension.

FIGURE 11. Optimal results for the Ankle Dorsi/Plantarflexion.

C. FRAMEWORK OF THE ROBUST DESIGN BASED ON THE AWPA

The framework based on the AWPA for the robust design can be described as follows.

Step 1: *Define the robust design model*. Design variables are expressed by the vector $\mathbf{X} = [x_1, \cdots, x_{10}] = \left[\bar{\beta}_1\left(t_{hi}\right), \cdots, \bar{\beta}_5\left(t_{hi}\right), \hat{\beta}_1\left(t_{hi}\right), \cdots, \hat{\beta}_5\left(t_{hi}\right)\right]$; the objective functions are $f_1\left(\cdot\right)$ and $f_2\left(\cdot\right)$; the consistency between the actual and targeted position of the end-effector is the constraint functions.

Step 2: *Initialization*. Set up the initial parameters of the AWPA and create the first-generation population.

Step 3: *Construct the robustness index*. Considering the CGA data as the target, the robust index is constructed.

Step 4: *Fitness evaluation*. With the objective functions, the fitness values are evaluated.

Step 5: *Criterion satisfaction*. If the termination criterion is satisfied, go to Step 8. Otherwise, go to the next step.

Step 6: *Create the new population*. A new population is created by the following operations: *Scouting, calling*, and *Besieging*.

Step 7: *Loop*. Return to Step 3 with the new population for the next generation.

Step 8: *End*. Output the optimal results.

Step 9: *Results analysis*. The optimal results will be analyzed and smoothed for realizing the consistency with the practical motion of human walking.

The flowchart of the robust design based on AWPA is schematically depicted in Figure 5. Generally, an engineer can make trade-offs within this set under practical requirements by focusing the set of Pareto front choices, which provides a visualized demonstration of the Pareto-optimal solution, but with an unclear indication of optimal diversities for decision-making. As given in Figure 6, it utilizes the fast approach of Pareto-optimal solution recommendation (FPR) using the Pareto risk index (β_2) [25], which provides users with a recommendation list of optimal ranking and optimal trend indications with different risk tolerance.

As shown in Figure 6, the FPR workflow can be summarized as the following 7 steps:

- Step 1: start the program;
- Step 2: build fitness function for multi-objective optimization, i.e., $[f_1, f_2, \cdots, f_N]$;
- Step 3: normalize the fitness function as $[f_1^0, f_2^0, \cdots, f_N^0]$;
- Step 4: calculate the PRI index β_2 using $[f_1^0, f_2^0, \cdots, f_N^0]$;
- Step 5: rank using β_2, as given in Eq. (28);

$$\beta_2\left(f\right) = \frac{\sigma_f}{\mu_f} \qquad (28)$$

- Step 6: calculate the evolutionary trend indices as the fitness function as given in Eq. (29), mean average precision (mmAP) and mean standard deviation (mmSTD) for β_2;
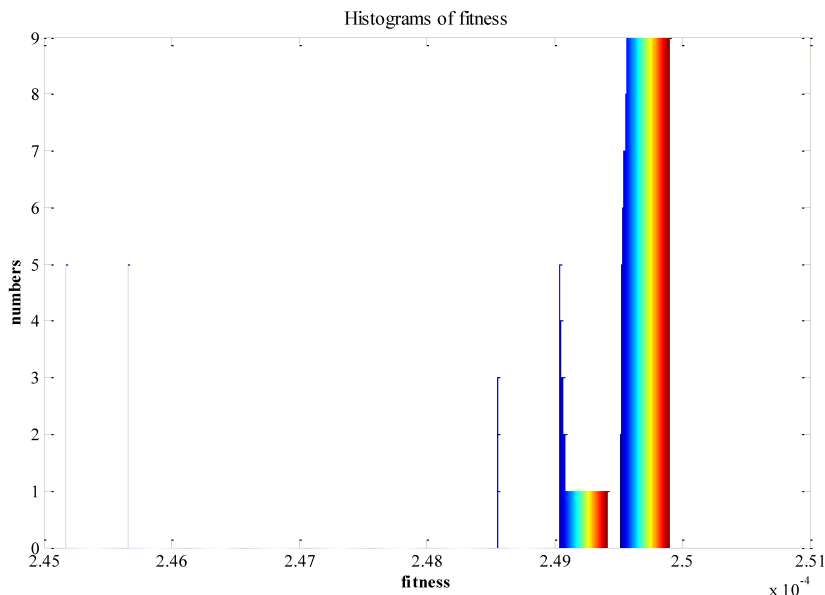
Z. Wang *et al.*: Robust Design for the Lower Extremity Exoskeleton Under a Stochastic Terrain by Mimicking WP Behaviors

IEEE *Access*

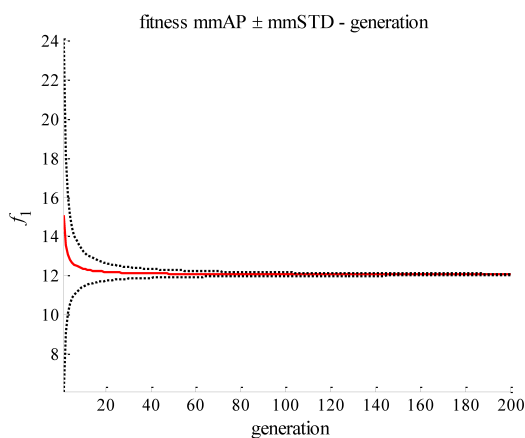**FIGURE 12.** Histogram of fitness for the ten times.

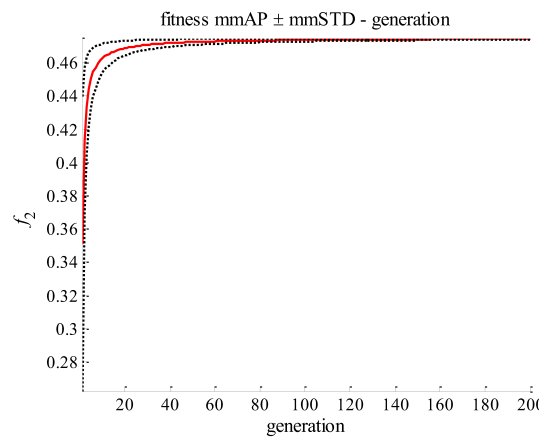**FIGURE 13.** Fitness mmAP ± mmSTD of f_1 over the generations.

FIGURE 14. Fitness mmAP ± mmSTD of f_2 over the generations.

So, the fitness function of this work can be expressed as:

$$F = maximise : mmAP[\beta_2(\|f_1\|, \|f_2\|)] \qquad (29)$$

▪ Step 7: terminate the program.

V. RESULTS AND DISCUSSIONS

The human dimensions stem from the Chinese standard "Human dimensions of Chinese adults", which are measured according to the Human ergonomics [24]. The main dimensions of Chinese adults are provided in Table 2. In this paper, we will take 1678 mm Male as a case and the thigh and leg length are 456 mm and 369 mm respectively.

Since the randomness from the stochastic terrain affects the performance during the stance phase, the robust design is implemented for the inverse kinematic problem during the stance phase and the deterministic design is used for

the inverse kinematic problem during the swing phase. The corresponding parameters for AWPA optimization are given in Table 3. The optimal results are shown in Figures 7-11 respectively. The blue curve is the mean of CGA data as the reference. The green curve is the optimal results for the inverse and the red curve is the smooth of the green curve for keeping the consistency with the practical motion. The upper and lower boundaries for 66.26%, 95% and 99% confidence intervals are also provided. From Figures 7-11, we can see (1) random motion of joints reacts the randomness from the stochastic terrain for keeping the consistence between the human and the lower extremity exoskeleton; (2) the optimal mean are very close to the mean of the CGA data and therefore the proposed methods are accuracy; (3) the motion of the Ankle Dorsi/Plantar flexion is most affected by the stochastic terrain and least for the motion of the Hip Flex/Extension;
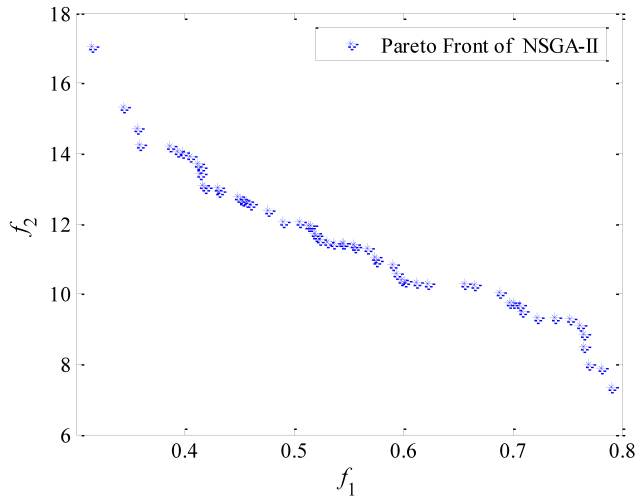
IEEE *Access*

Z. Wang *et al.*: Robust Design for the Lower Extremity Exoskeleton Under a Stochastic Terrain by Mimicking WP Behaviors

FIGURE 15. Pareto front of NSGA-II optimization.

TABLE 4. Comparison of accuracy and efficiency between NSGA-II and AWPA.

			Population	30	40	50	60
AWPA	Generation			150	150	180	200
	Objective	f_1		12	6.41	18.79	9.4868
		f_2		0.50	0.58	0.57	0.63
NSGA-II	Generation			1368	1920	5500	9400
	Objective	f_1		12	6.41	18.79	9.4868
		f_2		0.51	0.52	0.50	0.51

(4) under the given stochastic terrain, the probability that the practical motion is beyond the common motion is very small because the 99% confidence interval is within the interval between the upper and lower boundaries.

We use ten times to testify the robustness of the proposed framework based on AWPA for a given time point. The histograms of fitness are provided in Fig. 12. From Fig. 12, we can see the fitness for ten times lies between [2.49, 2.50] and furthermore nine times are the same.

As shown in Figs. 13 and 14, the red solid line is the moving mean of the average precision (mmAP) and the dashed lines are the moving mean of standard deviation (mmSTD) value of f_1 and f_2. It shows that the algorithm is converged nearly with 30 generations. The Pareto front of NSGA-II is provided in Fig. 15.

To make a comparison for NSGA-II and AWPA methods both in computational accuracy and efficiency, the generations and the objective function values are given in Table IV. The objective function value f_2 is determined from the Pareto front for NSGA-II under the same objective function value f_1 with that of the AWPA method. From Table IV, we can know the computational accuracy is similar while AWPA method has a higher computational efficiency.

VI. CONCLUSIONS

In this paper, we have developed a robust design method, which is novel for the lower extremity exoskeleton design. Within the validity of the simulations, optimal designs are achieved under a stochastic terrain by considering the effect of the stochastic terrain to the dynamic performance of the lower extremity exoskeleton via mimicking wolf packs. In achieving these, an inverse kinematic model for the lower extremity exoskeleton is first constructed by considering the stochastic terrain. The robust design model is then built for optimally assigning the randomness from the stochastic terrain to each joint. The optimization framework for the robust design based on the AWPA is thus completed. The results of the case study show that (1) the probabilistic consistency between the human and exoskeleton has been satisfied, such as that there is rare failure for each joint under the 99% confidence interval; (2) the optimization framework for the robust design is effective with high robustness and accuracy within the validity of simulations.

In future work, we shall enhance the exoskeleton design by developing time-variant robustness and reliability indices for capturing the time-varying and nonlinear performance of the exoskeleton during a dynamic waking cycle. Furthermore, the proposed AWPA algorithm will be embedded in the computational intelligence assisted design framework for physical prototyping, as sensors, actuators and controller chips for real-time control system applications are becoming standardized.

REFERENCES

[1] D. Tolani, A. Goswami, and N. I. Badler, "Real-time inverse kinematics techniques for anthropomorphic limbs," *Graph. Models*, vol. 62, no. 5, pp. 353–388, 2000.

[2] Z. Wang, X. Cheng, and J. Liu, "Time-dependent concurrent reliability-based design optimization integrating experiment-based model validation," *Struct. Multidiscipl. Optim.*, vol. 57, no. 4, pp. 1523–1531, 2018.

[3] S. Yu, Z. Wang, and K. Zhang, "Sequential time-dependent reliability analysis for the lower extremity exoskeleton under uncertainty," *Rel. Eng. Syst. Saf.*, vol. 170, pp. 45–52, Feb. 2018.

[4] Z. Wang, H.-Z. Huang, Y. Li, and N.-C. Xiao, "An approach to reliability assessment under degradation and shock process," *IEEE Trans. Rel.*, vol. 60, no. 4, pp. 852–863, Dec. 2011.

[5] R. Featherstone, "Position and velocity transformations between robot end-effector coordinates and joint angles," *Int. J. Robot. Res.*, vol. 2, no. 2, pp. 33–45, 1983.

[6] D. Manocha and J. F. Canny, "Efficient inverse kinematics for general 6R manipulators," *IEEE Trans. Robot. Autom.*, vol. 10, no. 5, pp. 648–657, Oct. 1994.

[7] J. U. Korein and N. I. Badler, "Techniques for generating the goal-directed motion of articulated structures," *IEEE Comput. Graph. Appl.*, vol. 2, no. 9, pp. 71–81, Nov. 1982.

[8] Z. Bingul, H. M. Ertunc, and C. Oysu, "Applying neural network to inverse kinematic problem for 6R robot manipulator with offset wrist," in *Proc. IEEE Int. Conf. Adapt. Natural Comput. Algorithms*, Coimbra, Portugal, Mar. 2005, pp. 112–115.

[9] A. T. Hasan, N. Ismail, A. M. S. Hamouda, I. Aris, M. H. Marhaban, and H. M. A. A. Al-Assadi, "Artificial neural network-based kinematics Jacobian solution for serial manipulator passing through singular configurations," *Adv. Eng. Softw.*, vol. 41, no. 2, pp. 359–367, 2010.

Z. Wang *et al.*: Robust Design for the Lower Extremity Exoskeleton Under a Stochastic Terrain by Mimicking WP Behaviors

IEEE*Access*

[10] R. Köker, "A genetic algorithm approach to a neural-network-based inverse kinematics solution of robotic manipulators based on error minimization," *Inf. Sci.*, vol. 222, pp. 528–543, Feb. 2013.

[11] J. A. Martin, J. de Lope, and M. Santos, "A method to learn the inverse kinematics of multi-link robots by evolving neuro-controllers," *Neurocomputing*, vol. 72, nos. 13–15, pp. 2806–2814, 2009.

[12] R. V. Mayorga and P. Sanongboon, "Inverse kinematics and geometrically bounded singularities prevention of redundant manipulators: An artificial neural network approach," *Robot. Auto. Syst.*, vol. 53, nos. 3–4, pp. 164–176, 2005.

[13] S. Tabandeh, C. M. Clark, and W. Melek, "A genetic algorithm approach to solve for multiple solutions of inverse kinematics using adaptive niching and clustering," in *Proc. IEEE Congr. Evol. Comput.*, Vancouver, BC, Canada, Jul. 2006, pp. 1815–1822.

[14] S. Momani, Z. S. Abo-Hannour, and O. M. K. Alsmadi, "Solution of inverse kinematics problem using genetic algorithms," *Appl. Math. Inf. Sci.*, vol. 10, no. 1, pp. 225–233, 2016.

[15] D. T. Pham, M. Castellani, and A. A. Fahmy, "Learning the inverse kinematics of a robot manipulator using the Bees algorithm," in *Proc. IEEE Int. Conf. Ind. Inform.*, Daejeon, South Korea, Jul. 2008, pp. 493–498.

[16] H.-C. Huang, C.-P. Chen, and P.-R. Wang, "Particle swarm optimization for solving the inverse kinematics of 7-DOF robotic manipulators," in *Proc. IEEE Int. Conf. Syst., Man, Cybern.*, Seoul, South Korea, Oct. 2012, pp. 3105–3110.

[17] J. L. Pons, *Wearable Robots: Biomechatronic Exoskeletons*, West Sussex, U.K.: Wiley, 2008.

[18] A. B. Zoss, H. Kazerooni, and A. Chu, "Biomechanical design of the Berkeley lower extremity exoskeleton (BLEEX)," *IEEE/ASME Trans. Mechatronics*, vol. 11, no. 2, pp. 128–138, Apr. 2006.

[19] W. Schiehlen and B. Hu, "Spectral simulation and shock absorber identification," *Int. J. Non-linear Mech.*, vol. 38, no. 2, pp. 161–171, 2003.

[20] N. Srinivas and K. Deb, "Multiobjective optimization using nondominated sorting in genetic algorithms," *Evol. Comput.*, vol. 2, no. 3, pp. 221–248, Dec. 1994.

[21] J. Horn, N. Nafpliotis, and D. E. Goldberg, "A niched Pareto genetic algorithm for multiobjective optimization," in *Proc. 1st IEEE Conf. Evol. Comput.*, vol. 1, Jun. 1994, pp. 82–87.

[22] K. Deb, S. Agrawal, A. Pratap, and T. Meyarivan, "A fast elitist non-dominated sorting genetic algorithm for multi-objective optimization: NSGA-II," in *Proc. Int. Conf. Parallel Problem Solving Nature (PPSN), Parallel Problem Solving Nature PPSN VI*, 2000, pp. 849–858. [Online]. Available: https://link.springer.com/chapter/10.1007%2F3-540-45356-3_83

[23] Y. Chen, Z. Wang, E. Yang, and Y. Li, "Pareto-optimality solution recommendation using a multi-objective artificial wolf-pack algorithm," in *Proc. 10th Int. Conf. Softw., Knowl., Inf. Manage. Appl.*, Chengdu China, Dec. 2016, pp. 116–121.

[24] *Human Dimensions of Chinese Adults*, document GB10000-1988, Chinese State Bureau of Technology Supervision, Beijing, China, Standards Press of China, 1989.

[25] Y. Chen, B. Peng, X. Hao, and G. Xie, "Fast approach of Pareto-optimal solution recommendation to multi-objective optimal design of serpentine-channel heat sink," *Appl. Therm. Eng.*, vol. 70, no. 1, pp. 263–273, 2014.

[26] M. Seyedali, S. M. Mirjalili, and A. Lewis, "Grey wolf optimizer," *Adv. Eng. Softw.*, vol. 69, no. 3, pp. 46–61, 2014.

[27] L. Xi, T. Yu, B. Zhang, X. Zhang, and X. Qiu, "A wolf pack hunting strategy based virtual tribes control for automatic generation control of smart grid," *Appl. Energy*, vol. 178, pp. 198–211, Sep. 2016.

[28] C. Yang, X. Tu, and J. Chen, "Algorithm of marriage in honey bees optimization based on the wolf pack search," in *Proc. Int. Conf. Intell. Pervasive Comput.*, Jeju, South Korea, Oct. 2007, pp. 462–467.

[29] H.-S. Wu and F.-M. Zhang, "Wolf pack algorithm for unconstrained global optimization," *Math. Problems Eng.*, vol. 2014, Mar. 2014, Art. no. 465082.

[30] Y. Chen, Y. Mei, J. Yu, X. Su, and N. Xu, "Three-dimensional unmanned aerial vehicle path planning using modified wolf pack search algorithm," *Neurocomputing*, vol. 266, no. 29, pp. 445–457, 2017.

[31] S. Shoghian and M. Kouzehgar, "A comparison among wolf pack search and four other optimization algorithms," *World Acad. Sci., Eng. Technol.*, no. 72, p. 447, 2012.

[32] Q. Zhou, Y. Zhou, and X. Chen, "A wolf colony search algorithm based on the complex method for uninhabited combat air vehicle path planning," *Int. J. Hybrid Inf. Technol.*, vol. 7, no. 1, pp. 183–200, 2014.

ZHONGLAI WANG is currently a Professor of mechatronics engineering with the University of Electronic Science and Technology of China. He has served as a PI or Co-PI for over 10 research projects, including the National Science Foundation of China. He has published over 50 journal and conference papers, and has six authorized patents. His research interests mainly include system reliability modeling, reliability-based design optimization, robust design, and model validation. He was a recipient of the Ministry of Education of the Natural Science Award and the National Defense Science and Technology Progress Award. He has been selected as the Most Cited Chinese Researchers in safety, risk, reliability, and quality field for four times by Elsevier from 2014 to 2017.

SHUI YU is currently pursuing the Ph.D. degree in mechatronics engineering with the University of Electronic Science and Technology of China. He has published several journal and conference papers. His research interests include reliability analysis and design optimization, robust design, and the intelligent design optimization of robotic systems.

LEO YI CHEN (SM'17) received the B.Sc., M.Sc., and Ph.D. degrees. He has been taking a leading role in previous and current department to maintain multi-disciplinary research links, and develop external research collaborations both nationally and internationally. Also, he has been leading a few research grants with over 100 million lbs in the areas of artificial intelligence, high-performance computing, evolutionary computation, robotic systems, and also studies in multidisciplinary contexts. He has a high-level output of research publications in leading international journals and presentations at international conferences, which related to the research area of robotics, smart design and manufacture, and dynamics and artificial intelligence applications, e.g., palgrave communications, which demonstrates significant research and grant potential in engineering and cross-disciplinary applications. He is a member of AAAI, IET, AIAA, and ASME, and a fellow of HEA. He is also a Chartered Engineer. He is one of the editorial board members, and he has been one of the guest editors for five special issues.

YUN LI received the Ph.D. degree in parallel computing and control from the University of Strathclyde, Glasgow, U.K., in 1990. He was with the U.K. National Engineering Laboratory, East Kilbride, in 1989, and with Industrial Systems and Control Ltd., Glasgow, in 1990. He joined the University of Glasgow as a Lecturer in 1991 and later served as the Founding Director of the University of Glasgow Singapore. He is currently an Overseas Distinguished Professor with the Dongguan University of Technology, Guangdong, China, and a Professor in design, manufacture and engineering management with the University of Strathclyde. He is also a Chartered Engineer in U.K. He developed one of the world's first 30 evolutionary and neural computing courses in 1995 and the popular online interactive courseware GA_Demo for computer-automated design in 1997. He has over 260 publications, one of which is the most popular in the IEEE Transactions on Control Systems Technology and another the most cited in the IEEE Transactions on Systems, Man, and Cybernetics—Part B. In 1998, he established and chaired the IEEE Computer-Aided Control System Design Evolutionary Computation Working Group and the European Network of Excellence in Evolutionary Computing Workgroup on Systems, Control, and Drives for Industry. He is an Associate Editor of the IEEE Transactions on Evolutionary Computation and the IEEE Transactions on Emerging Topics in Computational Intelligence.

● ● ●